The Astronomical Journal, 159:272 (12pp), 2020 June https://doi.org/10.3847/1538-3881/ab8d42


# Hubble Space Telescope Astrometry in the Orion Nebula Cluster: Census of Low-mass Runaways

Imants Platais[1], Massimo Robberto[2], Andrea Bellini[2], Vera Kozhurina-Platais[2], Mario Gennaro[2], Giovanni Strampelli[2], Lynne A. Hillenbrand[3], Selma E. de Mink[4,5], and David R. Soderblom[2]
[1] Department of Physics and Astronomy, Johns Hopkins University, 3400 North Charles Street, Baltimore, MD 21218, USA; imants@jhu.edu
[2] Space Telescope Science Institute, 3700 San Martin Drive, Baltimore, MD 21218, USA
[3] Department of Astronomy, California Institute of Technology, Pasadena, CA 91125, USA
[4] Center for Astrophysics, Harvard-Smithsonian, 60 Garden Street, Cambridge, MA 02138, USA
[5] Anton Pannekoek Institute for Astronomy, University of Amsterdam, Science Park 904, 1098 XH, Amsterdam, The Netherlands
*Received 2019 October 21; revised 2020 April 15; accepted 2020 April 24; published 2020 May 21*

## Abstract

We present a catalog of high-precision proper motions in the Orion Nebula Cluster (ONC), based on Treasury Program observations with the Hubble Space Telescope's (HST) ACS/WFC camera. Our catalog contains 2454 objects in the magnitude range of $14.2 < m_{\rm F775W} < 24.7$, thus probing the stellar masses of the ONC from $\sim 0.4\,M_{\odot}$ down to $\sim 0.02\,M_{\odot}$ over an area of $\sim$550 arcmin$^2$. We provide a number of internal velocity dispersion estimates for the ONC that indicate a weak dependence on stellar location and mass. There is good agreement with the published velocity dispersion estimates, although nearly all of them (including ours at $\sigma_{v,x} = 0.94$ and $\sigma_{v,y} = 1.25$ mas yr$^{-1}$) might be biased by the overlapping young stellar populations of Orion A. We identified four new ONC candidate runaways based on HST and the Gaia DR 2 data, all with masses less than $\sim 1\,M_{\odot}$. The total census of known candidate runaway sources is 10—one of the largest samples ever found in any Milky Way open star cluster. Surprisingly, none of them have tangential velocities exceeding 20 km s$^{-1}$. If most of them indeed originated in the ONC, it may compel the re-examination of dynamical processes in very young star clusters. It appears that the mass function of the ONC is not significantly affected by the lost runaways.

*Unified Astronomy Thesaurus concepts:* Hubble Space Telescope (761); Space astrometry (1541); Proper motions (1295); Young star clusters (1833); Low mass stars (2050); Stellar dynamics (1596); Runaway stars (1417)

*Supporting material:* machine-readable table

## 1. Introduction

As one of the most recognizable objects in the astronomical sky and one of the most popular in studies of star formation, the Orion Nebula Cluster (ONC) may not need a formal introduction. Its basic properties are reviewed by, e.g., O'Dell (2001), O'Dell et al. (2008), and Muench et al. (2008). Over the past two decades, our understanding of the ONC has significantly improved, as evidenced by several hundred publications listed in the SIMBAD[6] astronomical bibliography. Our contribution to this huge body of various data for the ONC is a new set of relative proper motions obtained from a massive imaging effort by the Hubble Space Telescope (HST).

Until recently, there were only two studies (Jones & Walker 1988; van Altena et al. 1988) that provided accurate relative proper motions, albeit limited to stars brighter than $I \leqslant 16$ mag ($V \sim 20$). Both studies produced a clean sample of cluster members indicated by high membership probabilities: $P_{\mu} > 90\%$. The calculated proper-motion dispersion along one axis ranges from 0.76 mas yr$^{-1}$ to 1.18 mas yr$^{-1}$. Assuming that the ONC is at a distance of $414 \pm 7$ pc (Menten et al. 2007), this range of dispersions translates into velocity dispersions of 1.5 and 2.3 km s$^{-1}$. Both studies indicate a larger velocity dispersion in the $Y$-direction (south–north).

More recent contributions to the kinematics of ONC members are the studies by Kuhn et al. (2019) and Kim et al. (2019). The first of these studies analyzed Gaia DR 2 (Gaia Collaboration et al. 2018) proper motions in 28 young star clusters and associations. Among them, the ONC was given special attention due to its prominent role in our understanding of star formation. These authors found that the ONC is an ordinary gravitationally bound cluster, while the known asymmetry in the internal velocity distribution is re-confirmed. Similar conclusions were reached by Kim et al. (2019) using archival ONC images from various HST cameras and from ground-based Keck NIRC2 data, over a small field centered on the Trapezium.

These new proper-motion measurements have also stimulated searches of the objects likely ejected from the ONC (Kim et al. 2019; McBride & Kounkel 2019) and generated lists of potential low-mass runaways ($<1\,M_{\odot}$). Wang et al. (2019) performed $N$-body simulations, specifically designed to imitate the ONC, which indicate that, within 1 Myr, a few-body dynamical decay can eject a few massive OB stars. These simulations, however, do not address the low-mass escapees. The $N$-body simulations by Moyano Loyola & Hurley (2013) appear to be more universal, considering a variety of dynamical interactions between the stars and potential mechanisms for making the runaways at a large range of escape velocities and stellar masses. Over 4 Gyr, this study predicts a high percentage of slow-moving runaways.

The supremacy of Gaia absolute astrometry appears to be unassailable. Then, what is the contribution of our new relative proper motions? The strongest argument is that the Gaia limiting magnitude is at $G \sim 21$ mag, while HST can observe objects several magnitudes fainter. Another issue is the highly irregular nebulosity that forms a backdrop to the ONC and presumably adds semi-random noise to the Gaia measurements,

[6] http://simbad.harvard.edu/simbad/

effectively lowering the spatial resolution. In addition, the ONC contains objects whose apparent profiles significantly differ from those of the stars (e.g., protoplanetary disks dubbed as proplyds). As a result, such objects produce a poor fit by a standard stellar point-spread function. For such objects, we could utilize a template-fitting method developed specifically for HST images by Mahmud & Anderson (2008), but in practice, this is not feasible due to the low number of images. In general, the precision of a single positional measurement with HST is on a par with that of Gaia. All of these reasons make the HST data set on the ONC competitive with or even superior to small spatial fields.

We concentrate on the kinematic properties of ONC members via a new survey of proper motions. Astrometric measurements in this area are challenging. Therefore, we provide a detailed account on how to get from the centroids of objects to the catalog of proper motions (Section 2) and how they can be interpreted (Section 3). Our conclusions can be found in Section 4.

## 2. HST Surveys of Orion Nebula Cluster and Data Reductions

The Treasury Program on the ONC (GO-10246; PI: M. Robberto) produced a large number of observations with three different HST cameras through 10 different filters (Robberto et al. 2013). The main purpose of this program was to obtain photometry in various bandpasses over a contiguous area of the sky in order to characterize all detected sources such as stars, circumstellar disks, proplyds, and brown dwarfs. In the region of the ONC, the spatial density of the sources is intrinsically low. If we consider the HST imaging instrument with the largest field of view (FOV) covering ∼11 arcmin$^2$—the Wide-Field Channel of the Advanced Camera for Surveys (ACS/WFC)—then even in the Trapezium area, a single long exposure can only detect ∼300 sources with a signal-to-noise ratio above 5. The number of detected sources quickly drops to ∼50 or fewer outside the Trapezium. Many of these sources are not appropriate for high-precision astrometry (especially proplyds), which further reduces the number of available "astrometric" stars.

This first HST Treasury Program on the ONC was done over two sets of epochs, 2004 October 11–November 7 and 2005 March 3–April 26, with a ∼180° change of the HST orientation between these periods. These two sets of observations constitute our first epoch. In order to achieve complete spatial coverage with two cameras, ACS/WFC and WFPC2 (the Wide-Field and Planetary Camera 2), the observations were acquired along nine strips oriented close to the east–west direction so that, for the ACS/WFC, there is a ∼50% overlap between adjacent pointings in this direction. The drawback of this observing strategy is a small and variable 5%–40% overlap in the south–north direction (see Figure 2 in Robberto et al. 2013). Such a limitation is undesirable for the construction of an astrometric reference frame, if we have to rely entirely on HST observations (e.g., Platais et al. 2015).

A decade later, we designed a second HST Treasury Program on the ONC (GO-13826; PI: M. Robberto) that addresses some of the shortcomings listed above. For the purpose of deriving proper motions, the ACS/WFC observations were designed to reproduce—to the extent possible—the same pointings and exposure time, telescope orientation, guide stars, and the Earth-orbit position as in our first survey. In order to optimize the telescope time, we used only the primary pointings (visits, a total of 52) in program GO-10246 and ignored all of the 50%-offset pointings. The necessary overlap between adjacent pointings and strips was achieved by adopting larger dithers. Only the broadband filter F775W was used for these observations over two time periods in 2015 February 8–April 28 and 2015 August 1–October 29, thus establishing our second epoch. We note that, due to the problems related to finding appropriate guide stars, four visits have a significant spatial offset with respect to the corresponding GO-10246 first-epoch pointings, and 17 visits have a slightly different roll angles.

In what follows, we used only the ACS/WFC images taken through filters F775W and F555W. These ACS/WFC filters are well-calibrated astrometrically, provide a similar saturation level and limiting magnitude, and sample the ONC area equally in both Treasury Programs. We employed all available 340–385 s exposures as well as all 8 s exposures that contain a reasonably high number of stars. This amounted to 196 first-epoch images and 259 second-epoch images. From the Mikulski Archive for Space Telescopes, we downloaded the bias-subtracted, dark-subtracted, flat-fielded, and corrected for charge transfer inefficiency `_flc.fits` files. We used the software code `img2xym_WFC.09x10` (Anderson & King 2006) to calculate precise positions and instrumental magnitudes for all detectable sources and a quality-of-fit (`qfit`) parameter.

### 2.1. Geometric Distortion Corrections

A standard reference for the geometric distortion of the ACS/WFC is provided by Anderson (2007), with additional improvements provided by Úbeda et al. (2013). However, a recent astrometric study on the region of 30 Dor (Platais et al. 2015) indicates that the existing corrections can be further improved. This prompted us to obtain a new set of corrections based on the extensive new study of the geometric distortion of the ACS/WFC (Kozhurina-Platais et al. 2015). The principal difference between the previous work by Anderson (2007) and that of Kozhurina-Platais et al. (2015) is the separation of the fine-scale distortion of the detector (lithographic-mask pattern) from the filter-dependent distortion in the latter study. Still, the study by Kozhurina-Platais et al. (2015) is limited by the accuracy of the original HST standard astrometric catalogs. This issue has been addressed by Kozhurina-Platais et al. (2018) using Gaia Data Release 1 (DR 1; Gaia Collaboration et al. 2016). The authors show that the original HST standard catalogs are affected by measurable differences in rotation and scale with respect to Gaia DR 1 and also contain a small uncorrected skew term. We implemented the necessary upgrades to the existing astrometric standard for the globular cluster 47 Tuc so that it is now on the system of Gaia DR 1. Then, the improved astrometric standard catalog was used to recalibrate the distortion solutions for the ACS/WFC F555W and F775W filters at both epochs of our ONC observations. With the new set of constants and look-up tables accounting for a total of four separate components in the ACS/WFC geometric distortion (correlated detector-grid imperfections, tiny filter flaws, polynomial part of distortion, and the time-dependent skew correction), we expect our measured positions of a single image to be accurate at a level of 2–3 mas. For the ONC region, this is crucial because the small number of reference stars per image prevents us from using the so-called

local solutions to calculate the proper motions, which are largely immune against the imperfect geometric distortion corrections.

### 2.2. Setting up the Astrometric Reference Frame

The sky area in the direction of the ONC is very complex: a bright and patchy nebulosity, the presence of bright stars, and the intrinsically low number of stars. Such conditions are not favorable for high-accuracy astrometry with HST over the small FOV of its imaging instruments. Gaia is expected to provide a major improvement to the absolute astrometry in this area. Nevertheless, the HST contribution is essential at fainter magnitudes, beyond the Gaia detection limit. For this, we need to construct an astrometric reference frame that serves as a "touchstone" to our selected 455 ACS/WFC images of the ONC.

Our initial choice was to base the reference frame on the VISTA Orion A Survey (Meingast et al. 2016), a deep near-infrared survey that contains ∼40 counterparts per single ACS/WFC image within our FOV. The epoch of the VISTA survey near the ONC is 2013.2, which is reasonably close to our second epoch. This makes the VISTA survey a suitable candidate for the astrometric reference frame, once the positions of stars are translated into the Gaia system. Then, each second-epoch ACS/WFC frame can be transformed into the revised VISTA coordinates by using least-squares and a polynomial model. The typical residuals of this coordinate transformation are on the order of ∼20 mas. Next, we followed closely the procedures to compute proper motions, described in detail by Platais et al. (2018). However, the resulting preliminary proper motions of the ONC objects showed a ∼20% larger internal velocity dispersion (IVD) than those of existing studies (e.g., Jones & Walker 1988). Apparently, the existing ground-based observations over spatial scales exceeding ∼1′ may not produce an adequate positional precision to support astrometry from HST without a significant loss of accuracy. Therefore, we had no viable alternative but to construct an astrometric reference frame directly from the HST observations, since the available Gaia high-quality astrometry around the ONC is too sparse.

Once we have distortion-corrected positions with significant spatial overlap, a linear three-term transformation (offset, rotation, and scale) puts one set of positions (a tile) into the system of partially overlapping adjacent tiles. To construct the reference frame, only second-epoch observations and long exposures are used. These observations are better designed in terms of astrometry and also overlap chronologically with the Gaia measurements. Following the hierarchical accumulation algorithm by Platais et al. (2015), we chose an image of the Trapezium area (`jcol35inq`) as the seed of a global coordinate system for the ONC. In practice, a combination of heavy contamination from "bleeding" sources, numerous stellar impostors (see Figure 1), and a limited number of common stars between adjacent tiles (frequently less than 10) made some transformations possible only interactively. The distribution of the rms errors for all transformations is shown in Figure 2. The majority of rms errors are concentrated at ∼0.02 pixel, equivalent to 1 mas on the sky. This is comparable to the rms scatter listed for the ACS/WFC observations in the 30 Doradus region (Table 2; Platais et al. 2015), despite a huge difference in the number of available common stars. None of our transformations are based on more than 60 stars. As a result, we obtained a catalog of 10,409 sources in our area of the ONC, which is a mixture of real stars, other celestial objects, and all kinds of spurious objects. In order to align the catalog along the R.A. and decl. axes, it is rotated by 82.°2309. These rotated *XY* coordinates provides our astrometric reference frame in units of the ACS/WFC distortion-corrected pixels.

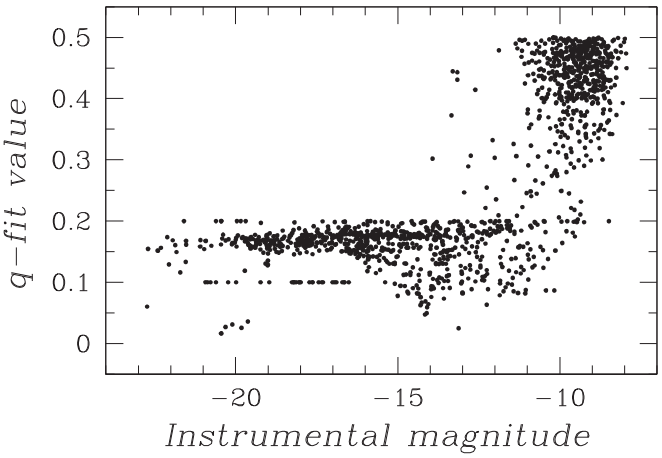


**Figure 1.** Distribution of the quality parameter `qfit` for sources measured in the central ONC image `jcol35inq`. Only a small fraction of detections with instrumental magnitudes brighter than −16 are stars and other sources.

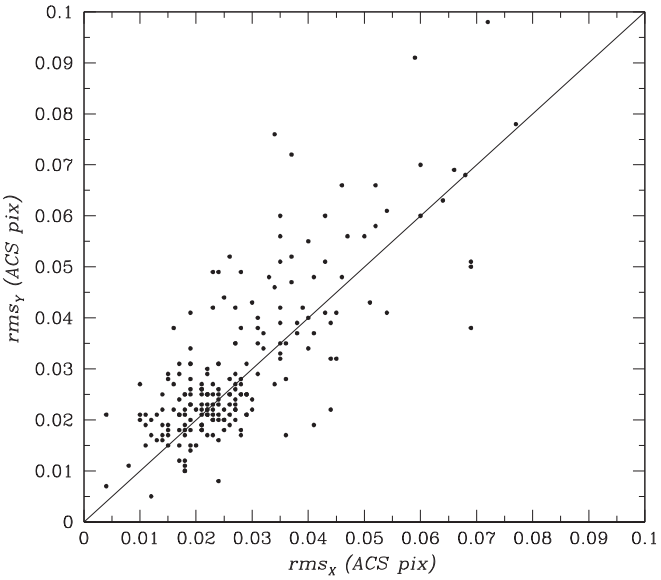


**Figure 2.** Distribution of rms errors from the least-squares transformations for all frame–tile, tile–strip, and strip–strip solutions. The nomenclature of these solutions is provided in Platais et al. (2015). The small number of common stars in several frame–tile solutions usually yields a high rms error.

In order to calculate equatorial coordinates of this astrometric reference frame, we used 452 stars from Gaia DR 2 and applied a linear three-parameter polynomial model in each coordinate. The resulting residuals indicate semi-gradual offsets up to ∼0.″07 across the FOV, equivalent to ∼1.4 ACS/WFC pixel. Such a pattern and the amplitude of these offsets were also noticed by Platais et al. (2018). In spite of our significantly improved corrections for geometric distortions, the nature of these offsets for the ACS/WFC is still an open question. We believe that the final Gaia astrometric catalog will help to eliminate this issue. In the following paragraphs, we

argue that the imperfections of an astrometric reference frame are not critical to our scientific results and their interpretation. If some portion of the final data catalog appears to be suspicious, then it is not used in our analysis or is marked in our catalog.

### 2.3. Proper Motions and Positions

The next step toward calculating proper motions is transforming all sets of pixel coordinates into the system of the astrometric reference frame (Platais et al. 2015). A linear three-parameter polynomial model in $X$ and $Y$ is used in the least-squares transformations. A notable difference between Platais et al. (2015) and our study is that we used combined sets of input coordinates, while in Platais et al. (2015), each ACS/WFC chip was transformed separately. This is also a default mode in applying the corrections for geometric distortion and is preferable when the number of stars is low. For our second-epoch observations, the solution's rms error is very small—at a level of 0.014 ACS/WFC pixel. However, similar first-epoch transformations produce much higher rms scatter—on average, 0.21 ACS/WFC pixel—due to the effect of proper motions over ∼10 yr. There are two potential issues with this. First, such a large scatter acts as a source of additional noise and, therefore, sets a limit to the final precision and accuracy of our relative proper motions. Second, in the case of a very low number of reference stars, $4 \leqslant n \leqslant 10$, that may bias the calculated proper motions, effectively reducing them. Fortunately, the pattern of our second-epoch pointings partially mitigates the impact of these issues. We note that the Gaia proper motions are immune to such effects, albeit they are still affected by nebulosity in the direction of the ONC.

The total number of first-epoch detections in the system of our astrometric reference frame is 42,000, while there are 136,000 second-epoch detections. The majority of the latter are hot pixels and cosmic rays. The detections in both epochs contain a large number of other artifacts such as "granulated" spikes of the brighter stars, especially near the Trapezium. In fact, the real detections are so polluted by these artifacts that we could not construct a reasonable global master list (such as in Section 3.3.1, Platais et al. 2015). Therefore, we adopted the ACS source catalog (Table 5, Robberto et al. 2013) as a clean and complete master list. The original equatorial coordinates of this catalog were translated into the Gaia DR 2 system by using the nearest nine common stars and their R.A. and decl. offsets. Then, the updated celestial coordinates were translated into the system of our astrometric reference frame.

Proper motions are calculated following the scheme outlined in Platais et al. (2015). Around each entry in the master list, we selected all detections (subsets) within a radius of 9 ACS/WFC pixels, equivalent to 450 mas. This size was chosen in order to find large proper motions in this area of the sky. On the other hand, it may be too large for calculating proper motion in the case of visual binaries and their components. Each detection has its estimated standard error based on the instrumental magnitude, thus allowing us to perform the weighted least-squares fit to the measurements in each coordinate as a function of time. We rejected the most deviant measurement, if its offset was larger than $4\sigma$. This extirpation is repeated, if necessary, until the lowest limit of measurements ($n = 3$) is reached (Platais et al. 2015). If an epoch has only two detections, then none of them are deleted. We caution that, in some of such cases, the resulting large proper motion might be spurious. A typical hint of such a failure can be a minimum number of data points in combination with significantly higher proper-motion errors. Our proper-motion catalog (Table 1) contains 2454 objects in the magnitude range of $14.2 < m_{\rm F775W} < 24.7$. The highest average precision of proper motions at 0.11 mas yr$^{-1}$ is obtained for objects in the magnitude range of $18.0 < m_{\rm F775W} < 21.0$ mag.

**Table 1**
Proper-motion Catalog

| Unit | Label | Explanations |
|---|---|---|
| … | ID | Number from Robberto et al. (2013) |
| mas yr$^{-1}$ | pmx | weighed proper motion in $X$ |
| mas yr$^{-1}$ | pmy | weighed proper motion in $Y$ |
| mas yr$^{-1}$ | e_pmx | error of the weighed proper motion in $X$ |
| mas yr$^{-1}$ | e_pmy | error of the weighed proper motion in $Y$ |
| … | cx | normalized $\chi^2$ for proper motion in $X$ |
| … | cy | normalized $\chi^2$ for proper motion in $Y$ |
| … | qx | goodness-of-fit probability $Q$ in $X$ |
| … | qy | goodness-of-fit probability $Q$ in $Y$ |
| mag | F775W | preliminary F775W magnitude |
| yr | ep_e | maximum extent of epochs |
| … | n1 | number of first-epoch data points |
| … | n2 | number of second-epoch data points |
| … | n_del | number of deleted data points |
| pix | max_res | largest residual in both proper-motion fits |
| pix | X | $X$-coordinate in ACS/WFC pixels aligned with R.A.[a] |
| pix | Y | $Y$-coordinate in ACS/WFC pixels aligned with decl. |
| deg | RAdeg | Right Ascension, decimal degrees (J2000) |
| deg | DEdeg | Declination, decimal degrees (J2000) |
| … | flag | reliability flag of selected proper motions |

**Note.**
[a] Direction of $X$-coordinate is opposite to R.A.
(This table is available in its entirety in machine-readable form.)

A low number of reference stars may produce very poor proper motions, especially near the edges of ACS/WFC frames, while all other astrometric parameters appear to be reasonable. Such cases would yield locally large and spurious proper motions. We conjecture that, within a small spatial spot, there should always be at least one object with a small proper motion. If this is not true, then the measured proper motion might be biased. Therefore, within 25″ around each fast-moving source, we examined the proper motions of surrounding sources. If there is at least one source with relatively small motion ($\mu \leqslant 2$ mas yr$^{-1}$) consistent with cluster membership, we assumed that the proper motion of a fast-moving source ($\mu \geqslant 5$ mas yr$^{-1}$) is reliable. Among the 141 such fast-moving sources, there are 26 possibly unreliable sources, all marked in the catalog.

In order to have an external check for our larger proper motions ($\mu \geqslant 4$ mas yr$^{-1}$; there are a total of 469 such objects), we used the astrometric information provided by Jones & Walker (1988), Gaia DR 2, and Kim et al. (2019). This exercise resulted in 64 sources with their proper motions confirmed at least by one independent data set, 15 sources with potentially unreliable proper motions, and 34 sources for which we found our measurement discrepant and, thus, marked accordingly. We also found 40 cases where the external source itself (including Gaia DR 2) has an unreliable proper motion. None of these objects with suspicious proper motions were used in the following analysis.

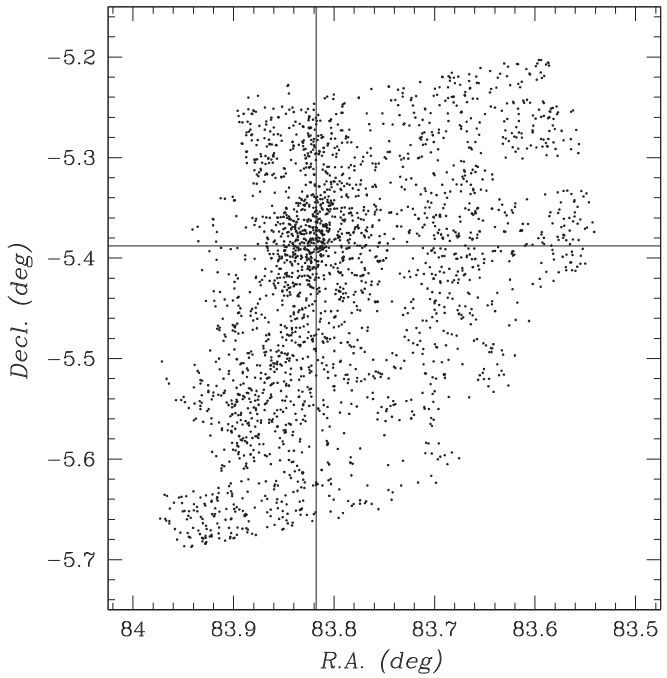


**Figure 3.** Spatial distribution of all sources with measured proper motions. The location of the Trapezium is marked by the crosshairs.

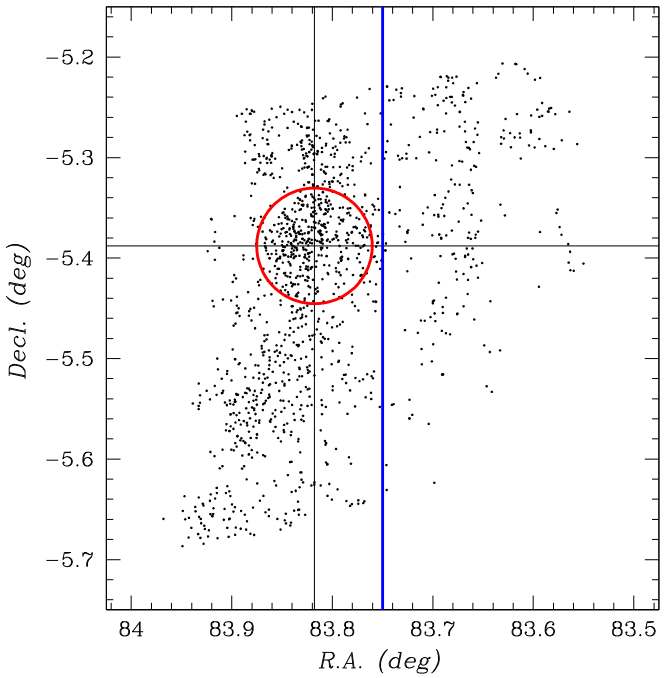


**Figure 4.** Spatial distribution of the selected 1379 sources with more reliable proper motions. Red circle: inner area of the ONC with a radius of 3.′45 centered on Trapezium; vertical blue line: cutoff at R.A. = 83.°75 separating the western sources with a possibly lower accuracy of proper motions.

## 3. Discussion and Applications

The primary objective of this project is to provide proper motions and the related tangential velocities for a large sample of low-mass stars in the ONC. The stars with measured proper motions cover an irregular area of $\sim$550 arcmin$^2$ with the approximate center at R.A. = $5^h35^m$ and decl. = $-5°27'$. We adopted the da Rio et al. (2014) center of the Trapezium as the center of the ONC (Figure 3). While the longest spatial extension of our field outwards from the Trapezium is $\sim$20′, in the east–north direction, it is significantly shorter (only $\sim$10′) and, thus, misses a substantial fraction of the ONC.

In order to mitigate detrimental effects of a small number of data points, we selected only those sources that have at least two data points at each epoch and have proper-motion errors smaller than 0.4 mas yr$^{-1}$. There are a total of 1379 sources with such properties, and *only this sample is used in our analysis*. It should be noted that we probe a limited mass range of the ONC: from $\sim$0.4 $M_\odot$ down to $\sim$0.02 $M_\odot$, as estimated from the common sources with derived stellar parameters (Table 3, da Rio et al. 2012). Most likely, the majority of unused sources have reliable proper motions with the exception of those that have $\mu \geqslant 5$ mas yr$^{-1}$.

### 3.1. Internal Velocity Dispersion

An obvious application of our relative proper-motion catalog is a new estimate of the IVD for the ONC. Given a significant uncertainty in the distance of the ONC based on Gaia DR 2 data: 403 ± 7 pc (Kuhn et al. 2019) versus 389 ± 3 pc (Kounkel et al. 2018), we consider only tangential velocities expressed in mas yr$^{-1}$. In a typical star cluster, the first task would be to obtain membership probabilities. However, in the context of this study, the ONC is not an ordinary cluster. It is located approximately toward the Galactic anti-center and significantly away from the Galactic equator. The light from background stars is essentially blocked out by a dense molecular cloud. Effectively, these factors make the presence of field stars minimal. Next, due to the young age of the ONC, $\sim$2.5 Myr (da Rio et al. 2014), the color–magnitude diagram of low-mass pre-main-sequence stars is just a fuzzy band (Hillenbrand 1997; da Rio et al. 2012), exacerbated by a strong differential reddening (da Rio et al. 2012). Therefore, a membership selection based on the color–magnitude diagram alone could partially miss a sizeable number of genuine cluster members. Finally, the presence of confirmed runaway objects in the Orion Kleinmann–Low Nebula (Luhman et al. 2017; Rodríguez et al. 2017) and exotic accreting young stellar objects (YSOs; Manara et al. 2013) indicates that the use of traditional kinematic memberships (e.g., Jones & Walker 1988) may eliminate such extremely interesting sources. In the presence of these distinctive circumstances, we assume that all sources in our area of the ONC are members, as long as some other parameter (e.g., parallax) is not in obvious conflict with the cluster membership. This argument was also applied by Hillenbrand (1997) to infer the total mass of the ONC.

#### 3.1.1. New Estimates of IVD

The spatial distribution of our ONC objects is heterogenous, due to the layout of HST observations (Figure 3) and the light-blocking effects by nebulosity. Therefore, we defined two characteristic spatial structures: a circular area around the Trapezium and a south–north prolongation crossing the Trapezium. The radius of the former is 3.′45, equivalent to three times the core radius from the King model by Hillenbrand & Hartmann (1998) and Kuhn et al. (2019). The south–north prolongation is limited to the sources with R.A. $>$ 83.°75. Both features are marked in Figure 4. The next step is to set reasonable limits in the vector-point diagram of proper motions. Faster-moving sources are a mix of foreground stars, ejected objects from the ONC, and poorly measured proper

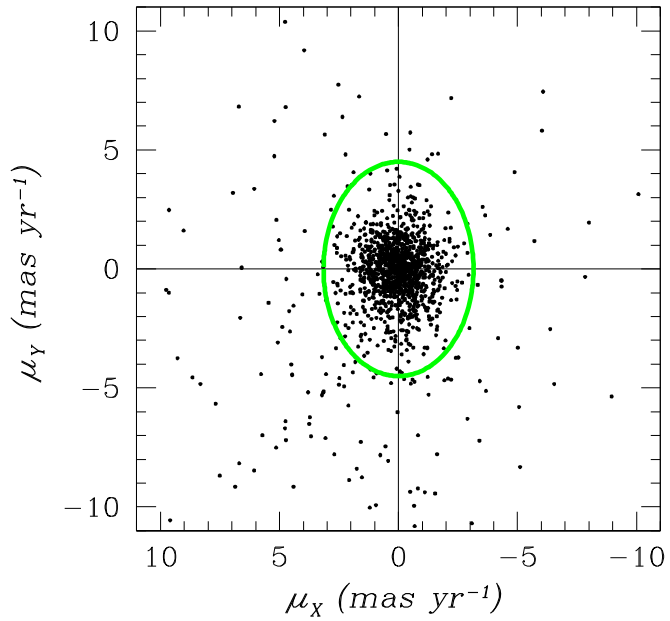


**Figure 5.** Vector-point diagram of sources shown in Figure 4. The green ellipse indicates the limit of selected proper motions used to calculate the internal velocity dispersion of the ONC.

motions. None of them should be contributing to the calculated IVD. Guided by the prior estimates of IVD, a relatively clean sample of the ONC members can be delineated by an ellipse with major and minor axes of 9.0 and 6.3 mas yr$^{-1}$, centered at $\mu_x = +0.04$ and $\mu_y = +0.08$ mas yr$^{-1}$ (Figure 5). This ellipse follows the velocity distribution along $\sim 3.5 \times \sigma_v$, where the subscript $v$ indicates the observed 2D proper-motion dispersion.

The IVD is calculated using the standard formulation (e.g., Jones & Walker 1988). For an estimate of the formal error, we used the method described in van der Marel & Anderson (2010), which takes into account individual uncertainties of proper motions. An additional contribution by likely systematic errors is not yet feasible to quantify.

The calculated IVD and its formal error for various samples of the ONC members are given in Table 2. In order to uncover a potential dependence of the IVD on stellar mass, we partitioned all subsamples at $m_{\rm F775W} = 20.0$ mag. Note that near the Trapezium (Figure 4, circular area), there is a clear shortage of very-low-mass objects. In part, this is a consequence of extreme contamination by various artifacts caused by the bright Trapezium stars. Variations of the IVD across the FOV and for different stellar masses are of the same order as our estimates of the IVD error. The angular asymmetry of the IVD is present at all stellar masses and locations. An elevated $\sigma_{v,x}$ for Sample 5 ($r > 3\farcm45$ and $m_{\rm F775W} > 20.0$) is puzzling. The only different parameter between the "brighter" and "fainter" samples is a significantly higher number of fainter sources at decl. $< -5\fdg45$. If we exclude these sources, then our global IVD estimate of the ONC is $\sigma_{v,x} = 0.94$ and $\sigma_{v,y} = 1.25$ mas yr$^{-1}$.

### 3.1.2. Complete List of Measured IVDs

Until recently, only two estimates of the IVD were available (Jones & Walker 1988; van Altena et al. 1988). Table 3 provides a significant addition, including our effort. It is not trivial to compare these estimates because of differences in the spatial and brightness coverage as well as due to the variety of reduction techniques for ground and space observations. It is expected that the final Gaia data will provide the best estimate of the IVD for sources more massive than $\sim 0.3\,M_\odot$. In turn, the HST is still the prime instrument for measuring proper motions of low-mass stars and brown dwarfs in the ONC. Within the errors, our study and that by Jones & Walker (1988) provide nearly identical IVDs. Note that, in Table 3, our estimate of the IVD is limited to the inner area around the Trapezium. The only outlier appears to be the $\sigma_{v,y}$ value obtained by van Altena et al. (1988). However, the internal kinematics of the brighter stars might be different than that of the low-mass stars.

There are two studies, by Kuhn et al. (2019) and Kim et al. (2019), which provide a somewhat lower IVD than those of other studies, including ours. It appears odd that largely the same HST observations used by us and Kim et al. (2019) can produce a ~7% smaller IVD in the latter study. On the other hand, Kim et al. (2019) expanded the time baseline to 20 yr (versus the 11 yr of this study) by including additional HST observations taken with other cameras through a variety of filters. Such favorable conditions—a longer time baseline and additional epochs—must significantly lower the proper-motion errors. However, Figure 6 shows the opposite; overall, for the 572 stars in common, the proper-motion errors by Kim et al. (2019) are significantly larger. If we calculate the IVD following the Jones & Walker (1988) formulation and applying the same spatial and magnitude cutoffs as in Section 3.1.1 but using the Kim et al. (2019) data and their errors, then the resulting formal dispersions along the $X$ and $Y$ axes, respectively, are 0.78 and 1.09 mas yr$^{-1}$. Assuming zero errors, the same dispersions are 0.85 and 1.15 mas yr$^{-1}$. This exercise demonstrates that larger proper-motion errors tend to lower the calculated IVD. Apart from the unusual distribution of proper-motion errors, there are no obvious clues to explain the likely underestimated IVD by Kim et al. (2019). The IVD estimate based on Gaia DR 2 (Kuhn et al. 2019) is consistent with other studies in the $Y$-direction but is significantly smaller in the $X$-direction. For the ONC area, this is consistent with significantly larger proper-motion errors along the R.A. in Gaia DR 2.

While working on potential runaway stars in the ONC, we conjectured that consideration should be given to another scenario. It is related to the north–south kinematic "stream" moving relatively fast across the ONC (see following Section 3.2). Most likely, this stream is part of the YSOs in the Orion A molecular cloud (Megeath et al. 2012). The proper motions of brighter ONC stars by van Altena et al. (1988) might be the least polluted by this stream and, in turn, their IVD estimate is more reliable given a similar size along *both* axes (Table 3). If indeed all other samples of ONC members are significantly contaminated, then one must somehow identify the true ONC members, that is, the objects dynamically associated with the Trapezium. Proper motions alone, no matter how accurate, cannot provide a clean sample of bona fide cluster members due to the intrinsically large IVD. Our proper motions indicate that possible kinematic differences in the tangential plane between the YSOs of Orion A and Trapezium are less than 0.1 mas yr$^{-1}$ and mainly in the $X$-direction. However, a study of the Orion A 3D shape (Großschedl et al. 2018) indicates that the bulk of its YSOs might be in the foreground of the ONC. A similar argument is provided in Appendix A of Kuhn et al. (2019). We believe that the final Gaia parallaxes will decisively separate these two populations.

**Table 2**
Samples of Internal Velocity Dispersion in mas yr$^{-1}$

| Sample # | Area[a] | Magnitude Range | $\sigma_{v,x}$ | $\sigma_{v,y}$ | $N_{\rm stars}$ |
|---|---|---|---|---|---|
| 1 | All | All | 0.94 ± 0.02 | 1.25 ± 0.03 | 1197 |
| 2 | $r < 3\farcm45$ | <20.0 | 0.91 ± 0.04 | 1.22 ± 0.05 | 293 |
| 3 | $r < 3\farcm45$ | >20.0 | 0.84 ± 0.06 | 1.20 ± 0.08 | 104 |
| 4 | $r > 3\farcm45$ | <20.0 | 0.91 ± 0.03 | 1.20 ± 0.04 | 361 |
| 5 | $r > 3\farcm45$ | >20.0 | 1.01 ± 0.04 | 1.32 ± 0.05 | 439 |
| 6 | East, $r > 3\farcm45$ | <20.0 | 0.89 ± 0.04 | 1.16 ± 0.05 | 300 |
| 7 | East, $r > 3\farcm45$ | >20.0 | 0.97 ± 0.04 | 1.33 ± 0.06 | 325 |

**Note.**
[a] Consult Figure 4 for the area conventions. "East" refers to a selection of sources eastward from R.A. = $83\fdg75$.

**Table 3**
Internal Velocity Dispersion in mas yr$^{-1}$

| Source | $\sigma_{v,x}$ | $\sigma_{v,y}$ | Spatial Extent | $N_{\rm stars}$ |
|---|---|---|---|---|
| van Altena et al. (1988) | 0.76 ± 0.09 | 0.83 ± 0.10[a] | radius = 30′ | 49 |
| Jones & Walker (1988) | 0.91 ± 0.05 | 1.18 ± 0.04 | 25′ × 30′ | 693 |
| Dzib et al. (2017) | 1.08 ± 0.07 | 1.27 ± 0.15[b] | 2′ × 2′ | 79 |
| Kuhn et al. (2019) | 0.73 ± 0.05 | 1.12 ± 0.10[c] | 20′ × 18′ | 48 |
| Kim et al. (2019) | 0.83 ± 0.02 | 1.12 ± 0.03 | 6′ × 6′ | 701 |
| This study | 0.89 ± 0.03 | 1.21 ± 0.04[d] | radius = $3\farcm45$ | 397 |

**Notes.**
[a] All stars brighter than $V = 12.5$ mag.
[b] From interferometric radio observations.
[c] Positional angle of 5° applied. In their notation, the pc2 axis is the $x$-axis (R.A.) as in all other studies.
[d] Approximately within the spatial area of Kim et al. (2019); a significantly lower number in our sample is due to the selection of reliable proper-motion measurements.

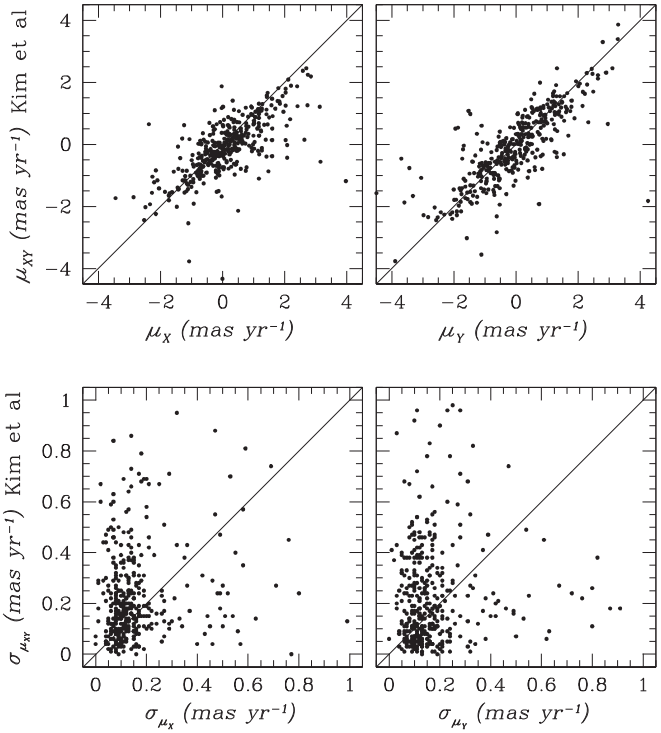


**Figure 6.** Comparison of proper motions and their errors between this study and that of Kim et al. (2019). While the proper motions are distinctly commensurate, the corresponding distributions of proper-motion errors are lopsided.

### 3.2. ONC Candidate Runaways

The current status of potential runaway sources from the ONC is discussed in McBride & Kounkel (2019). They appear to cover the entire range of spectral types from O9.5 V down to late M stars. Following earlier attempts to identify runaway objects from the ONC, such as Tan (2004), Poveda et al. (2005), Kim et al. (2019), and McBride & Kounkel (2019), we explored various sets of proper motions for such objects. Considering that the ONC contains not only fully formed stars but also proplyds and protostars (e.g., the Becklin–Neugebauer object), here we adopt the short-hand term "runaway" to characterize all sources and objects in the process of being ejected from the ONC regardless of the escapee's velocity. One way to identify such objects in the ONC is to use the virial theorem and the estimate of the mean-square escape velocity at ∼3.1 mas yr$^{-1}$ (5.9 km s$^{-1}$, assuming a distance of 400 pc), beyond which an object is classified as a runaway (Kim et al. 2019). We complemented this approach with an additional constraint by adding the vectorial angle between the proper motion with respect to the direction outward from the Trapezium (e.g., Platais et al. 2018). Given the importance of the Trapezium in various dynamical processes (e.g., Portegies Zwart 2016; Allen et al. 2017), it should also be a principal (but not the only one) engine for the production of runaways. We note that the spatial density of the potential runaways is proportional to the inverse of the squared distance from the Trapezium. In other words, the highest chance of finding a runaway by proper motions is near the cluster. In the following subsections, we discuss the status of runaways in five sets of proper motions.

#### 3.2.1. HST Treasury Programs of ONC (This Study)

We considered all sources with total proper motions larger than 5 mas yr$^{-1}$ and a total error less than 0.4 mas yr$^{-1}$. There are a total of 141 such sources (Figure 7). This figure shows how the vectorial angles are obtained and used to identify candidate runaways. In order to quantify the distribution of vectorial angles, we chose 13 bins with widths of $27\fdg7$. The bin size is optimized considering the errors of proper motions and the scatter of vectorial angles for some known candidate runaways. Figure 7 indicates a concentration of vectorial angles in the bin centered on $\Theta = 0°$, that is, where the potential Trapezium runaways are expected. At all other angles. the frequency of the stars should be flat, provided that the distribution of field-star proper motions is random. We note

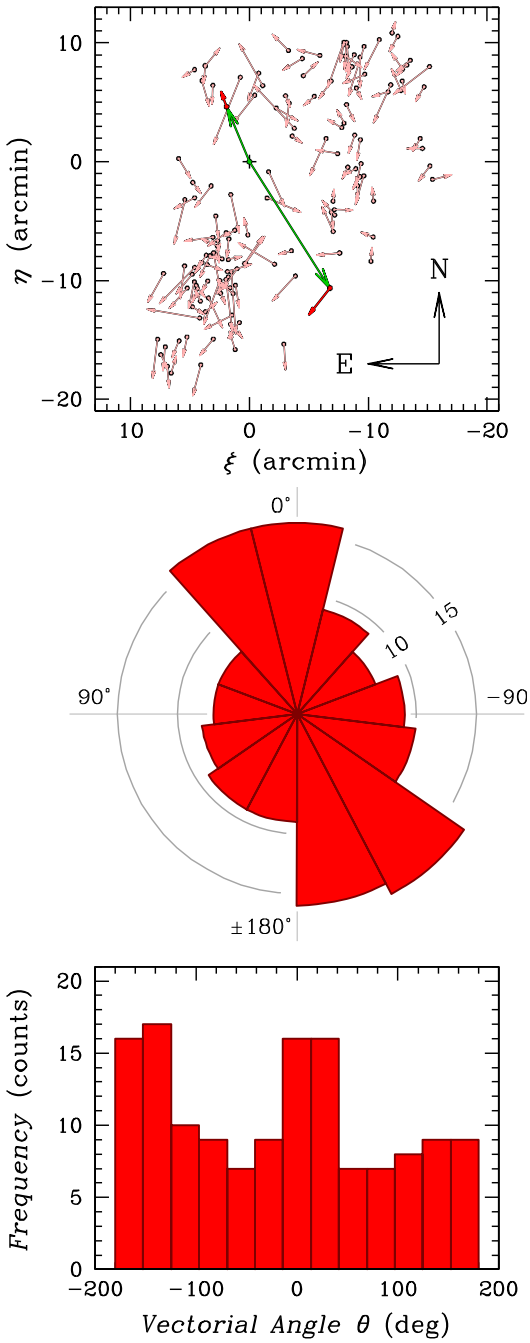


**Figure 7.** From a spatial map of the tangential velocities of the ONC to the 1D histogram of vectorial angles. Upper panel: a spatial distribution of 141 fast-moving sources and their proper motions in the tangential plane with the zero-point at the location of the Trapezium, marked by a small cross. The lengths of the arrows are proportional to the size of the proper motions. The vectorial angle between the position vector and the arrow of a proper motion is a key parameter to identify potential runaways. Position vectors (in green) are drawn to the location of two sources: a northern source has a very small vectorial angle $\Theta = -2.^{\circ}3$ and is a likely runaway candidate, while a southern source has $\Theta = -71^{\circ}$ and is a passing field star. Middle panel: polar histogram of vectorial angles for all sources in the upper panel. The bin size is $27.^{\circ}7$, and the upper bin is centered on $\Theta = 0^{\circ}$. The radial coordinate indicates the number of sources in each bin. Bottom panel: same as in the middle panel but transformed into the 1D histogram of vectorial angles. Only the central bin at $\Theta = 0^{\circ}$ contains likely runaways. The presence of other peaks is discussed in Section 3.2.1.

that a relatively large bin size may enable us to detect potential runways also originating from other massive stars and stellar systems of the ONC.

We noticed, however, an unusual excess of sources in the bins at $\Theta = -166^{\circ}$, $-138^{\circ}$, and $+28^{\circ}$. The majority of sources from the bin $\Theta = +28^{\circ}$ are located in the southeast quadrant (Figures 7, 8). In fact, these sources appear to have the same kinematic pattern as the sources in the bins at $\Theta = -166^{\circ}$, $-138^{\circ}$ that are $\sim 180^{\circ}$ apart and located in the northwest quadrant. We interpret this pattern as the presence of a stellar stream running approximately north–south. The distribution of the proper-motion vectors in polar coordinates of our 141 fast-moving sources indicates the dominant direction toward $\varphi = 162^{\circ}$ (from north to east) with the associated Gaussian FWHM $= 68^{\circ}$ (Figure 9). These parameters very well describe the pattern visible in the histograms (Figures 7, 8; left upper panel). All four peaks are mainly due to the field stars streaming across the ONC. Our kinematic data alone cannot be used to identify potential runaways because of dominating background stars. Even more, an equal number of sources in the bins at $\Theta = 0^{\circ}$ and $+28^{\circ}$ effectively rules out the presence of runaways in our data set. As a result, we single out only source #7320 (Table 4), the proper-motion error of which only slightly exceeds the adopted precision threshold but formally has the smallest vectorial angle among all fast-moving stars.

One of the most reliable censuses of the low-mass ONC members down to $\sim 0.02\,M_{\odot}$ was produced by da Rio et al. (2012). This study used empirical relations to determine effective temperature $T_{\rm eff}$ and total extinction $A_V$ from optical colors. These parameters were used to construct the Hertzsprung–Russell diagram and, then, to identify likely cluster members. We cross-correlated the list of these cluster members with our proper-motion catalog and examined the vectorial angles adopting the same parameters as above. There are a total of 819 common sources, including 17 common fast-moving objects (Figure 8; upper right panel). Statistically, the distribution of vectorial angles implies a single field object and four candidate runaways. We selected three sources as our best sample of potential runaways within the mass range of 0.11–0.35 $M_{\odot}$, all having impact parameters less than $50''$ (Table 4), well aware that the same sources contributed to the histogram of all fast-moving objects (Figure 8; upper left panel). The estimated standard error of the vectorial angles for these candidate runaways is $\sim 0.^{\circ}5$, and their total proper motions span from 6.8 to 9.8 mas yr$^{-1}$, equivalent of 13.3 to 19.2 km s$^{-1}$.

Summarizing our contribution to the subject of ONC runaways, we acknowledge that it is ambiguous. For example, if the authors of the low-mass ONC-member list (da Rio et al. 2012) would have had access to our proper motions, then all of our fast-moving sources could be classed as background objects (see; da Rio et al. 2010). This conundrum necessitates a complex study of each candidate runaway; high priority should be given to obtaining a set of key astrophysical parameters. If they match those of the bona fide cluster members, then the likelihood of being a former cluster member would be irrefutable.

We noticed a Trapezium-like configuration among the fast-moving low-mass field objects comprising #1115, 1127, 1167, and 1169. Their mutual separation is about $15''$, and three of them are co-moving. The kinematics of these objects is not compatible with the ONC membership nor a runaway status. As expected, none of them are listed in da Rio et al. (2012). Nonetheless, it is an interesting case in terms of the formation and stability of such systems.

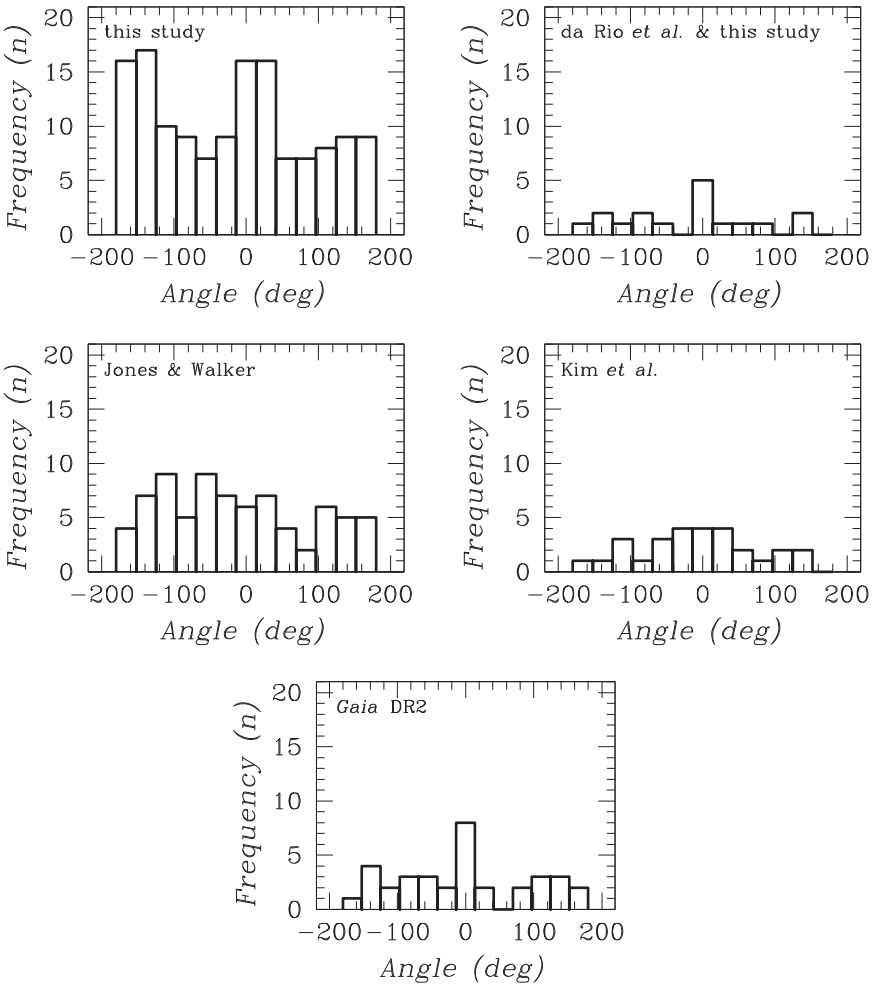


**Figure 8.** One-dimensional histograms of vectorial angles for sources with larger proper motions. The source (authors) of proper motions is indicated in each panel. A significant excess of sources at a zero angle in three of the five histograms indicates the presence of runaway sources. A detailed analysis is given in Section 3.2.

Finally, we briefly explored whether, besides the Trapezium, some other massive ONC members (Table 4, Muench et al. 2008) can produce additional candidate runaways. Inside the circle ($r = 8'$) centered on the Trapezium, there are five such stars—Brun 655, 682, 714, 747, and 760. All of them produce vectorial-angle histograms similar to that in Figure 8 (upper left panel), with a significant amount in the bin $\Theta = 0°$ and a heavy spatial concentration in the southeast quadrant. Similar to the case of the Trapezium, it is not possible to identify reliable runaways. However, we note that Brun 747 is a massive hierarchical triple system (Shultz et al. 2019) capable of ejecting a cluster member.

### 3.2.2. Jones & Walker (1988)

A relatively deep survey of the ONC proper motions by Jones & Walker (1988) can, in principle, be used to search for runaways. Poveda et al. (2005) suggested three runaways (also known to be the proplyds) among this set of proper motions, a claim that was disproved (O'Dell et al. 2005). We confirm that these objects do have small proper motions and cannot be astrometric runaways. There are a few other cases of inflated proper motions and/or underestimated membership probabilities in the Jones & Walker catalog (see Hillenbrand 1997), likely due to the effects of partially resolved visual binaries. The distribution of the proper-motion vectorial angles of fast-moving stars (Figure 8) is inconclusive about the presence of potential runaways. Among the formal six potential runaways, source JW 45 appears to be the only candidate runaway confirmed by Gaia DR 2.

### 3.2.3. Kim et al. (2019)

The analysis of proper motions by Kim et al. (2019) was one of the first attempts to identify escaping cluster members among the high-velocity stars that are habitually classified as background sources. These authors adopted an angular escape velocity of 3.1 mas yr$^{-1}$, above which a star can be considered escaping from the ONC. We found that, in the group of high-significance escapers (ESC 1), sources Kim 209 and 232 have significantly smaller proper motions in our catalog. If we calculate the vectorial angle, then only Kim 572, 611 and 713 appear to have had a close encounter with the Trapezium. None of them are in our catalog. The histogram of vectorial angles (Figure 8) indicates one to two potential runaways. Source Kim 713 is the Becklin–Neugebauer object BN—a well-known escapee from the ONC area (Rodríguez et al. 2017).

### 3.2.4. Gaia DR 2

There is a very limited overlap between the HST candidate low-mass runaway sources and the potentially brighter

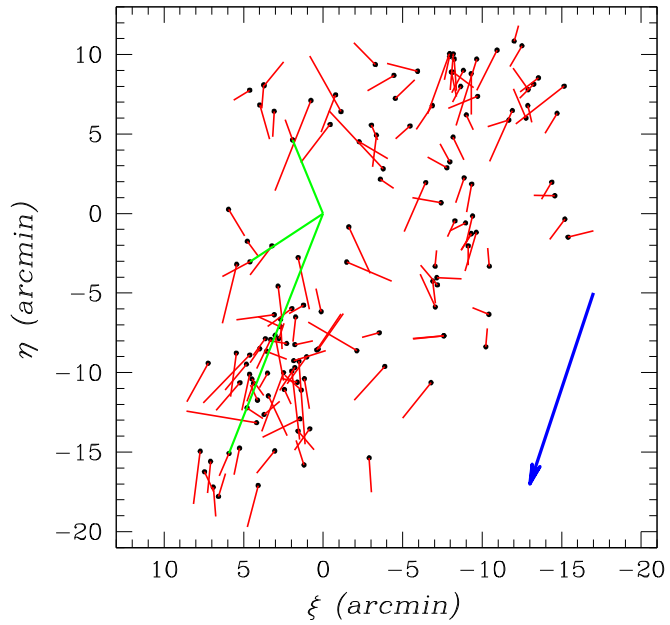


**Figure 9.** Spatial distribution of our faster-moving sources. Proper-motion vectors are shown by the red line segments at a scale of 5 mas yr$^{-1}$ per 1′. The total proper motions range from 5 to 30 mas yr$^{-1}$. Three green lines with their origin at the Trapezium indicate new low-mass candidate runaways from our *HST* Treasury programs of the ONC. The blue arrow shows the dominant direction of Orion's A faster-moving young stellar objects.

**Table 4**
Candidate Low-mass Runaways from ONC

| Ident | F775W (mag) | $X$ (arcmin) | $Y$ (arcmin) | Total PM (mas yr$^{-1}$) | Angle (deg) | $d$ (″) |
|---|---|---|---|---|---|---|
| 6177 | 17.603 | 1.9207 | 4.6279 | 6.81 | −2.3 | 12 |
| 7320[a] | 23.369 | 4.0906 | −17.0977 | 13.50 | −1.0 | 18 |
| 7495 | 21.721 | 4.6063 | −3.0388 | 9.79 | −5.6 | 33 |
| 7863 | 22.077 | 5.9075 | −15.0817 | 7.74 | −2.0 | 33 |

**Note.**
[a] Not a counterpart in the ONC-member list by da Rio et al. (2012). The last column shows the extrapolated nearest angular distance from the Trapezium (impact parameter).

runaways in Gaia DR 2. However, runaways are expected over a wide range of masses, not only in the low-mass domain.

In order to mimic our FOV, we selected DR 2 stars within 20′ of the Trapezium with a total proper motion larger than 4 mas yr$^{-1}$ and a total error $\sigma_\mu < 0.55$ mas yr$^{-1}$. The absolute proper motions from DR 2 were translated into the system of our relative proper motions. Initially, we considered all Gaia stars with parallaxes $1.9 < \varpi < 3.1$ mas. Within these specifications, there are 35 fast-moving stars. This range of $\varpi$ still comprises a large distance range, between 320 and 530 pc. Probing a clean sample of ONC members along the line-of-sight direction would require that the parallax errors be no larger than ∼0.03 mas, while the current sample has an average parallax error of 0.1 mas.

The histogram of the vectorial angles for our selection of DR 2 stars shows a convincing peak in the zero bin (Figure 8) and, thus, reinforces our conclusions on the ONC runaways. Statistically, it indicates a total of six runaways. However, a lesson learned from our HST proper motions (Section 3.2.1) compels us to narrow the range of well-measured parallaxes within $1\sigma$ around the average $\varpi = 2.50$ mas. This cutoff eliminates nearly all potential runaway candidates in the controversial southeast quadrant and produces four likely runaway candidates (Table 5 and Figure 10). There is one visual binary: sources #1 and #2 are at a spatial separation of 17.″7, but they cannot be a physical pair due to the $\sim 10\sigma_\mu$ difference in proper motions. This pair is also discussed by McBride & Kounkel (2019). In fact, Table 5 contains only one new candidate runaway that is not listed by McBride & Kounkel (2019). This is source #1 = JW 45 (see Section 3.2.2) = Parenago 1540 (Marschall & Mathieu 1988). It is a pre-main-sequence double-lined spectroscopic binary. Marschall & Mathieu (1988) were the first to propose that Parenago 1540 might be a runaway from the Trapezium. The Gaia DR 2 data clearly support this proposition.

### 3.2.5. McBride & Kounkel (2019)

A new study of runaway young stars near the ONC (McBride & Kounkel 2019) is conceptually closest to our approach. These authors used a sample of Gaia DR 2 data within a radius of 2° around the Trapezium. The most interesting part of this study is their proposed sources originating from the Trapezium. There are nine such sources. Among them, three (sources *a*, *b*, and *g*) are in common with our selection of runaways in Gaia DR 2 (Table 5). Source *e* has a large impact parameter at ∼9′, indecisive Gaia astrometry, and is located in the controversial southeast quadrant. Similarly, source *c* has poor Gaia astrometry and a larger impact parameter, incompatible with the origin in the Trapezium. In turn, source *d* has a $4.5\sigma$ parallax offset from the mean ONC parallax provided by Kuhn et al. (2019), thus, indicating a background object. If we exclude these three sources, then these authors have contributed a total of six new candidate runaways out to ∼1° around the Trapezium. A caveat to this list is a strong spatial alignment along the north–south direction, which mimics the distribution of fast-moving field YSOs in our data (Figure 9).

### 3.2.6. Census of ONC Runaways

In summary, our HST ACS/WFC study alone produced three new ONC candidate runaways in the magnitude range $17.6 < m_{\rm F775W} < 22.1$ mag. The status of an additional source 7320 is not clear (see Section 3.2.1); therefore, it is omitted in this census. In addition, we propose one new Gaia DR 2 candidate runaway at $G = 10.8$ mag. Formally, the enigmatic Orion BN object can be classed as an ONC runaway; however, it seems to be a member of a multiple system in the Orion Kleinmann–Low Nebula (e.g., Luhman et al. 2017; Rodríguez et al. 2017). This scenario is partially weakened by the failure to detect water vapor in close proximity to BN (Indriolo et al. 2018). Given the unclear status of BN, we ignore it in our census.

Considering the additional six runaways identified by McBride & Kounkel (2019), the current census of ONC runaways includes a total of 10 candidates. However, considering the caveats to various data sets, our census may still contain ∼50% impostors. By the same token, we may have overlooked some additional genuine runaways. The range of equivalent tangential velocities for all of these candidate

**Table 5**
Likely Escaped Stars from ONC in Gaia DR 2

| Ident | R.A. (DR 2) (deg) | Decl. (DR 2) (deg) | $\varpi$ (mas) | $G$ (mag) | $X$ (arcmin) | $Y$ (arcmin) | Total PM (mas yr$^{-1}$) | Angle (deg) | $d$ ($''$) |
|---|---|---|---|---|---|---|---|---|---|
| 1 | 83.66566645 | −5.40711238 | 2.495 ± 0.043 | 10.818 | −9.0844 | −1.1545 | 5.24 | −3.3 | 32 |
| 2[a] | 83.61391001 | −5.40619446 | 2.546 ± 0.041 | 11.609 | −12.1760 | −1.1003 | 8.55 | −1.8 | 23 |
| 3[a] | 83.60906346 | −5.40527690 | 2.519 ± 0.044 | 12.713 | −12.4656 | −1.0454 | 7.25 | −1.2 | 16 |
| 4[a] | 83.76792173 | −5.13684069 | 2.431 ± 0.037 | 10.130 | −2.9777 | 15.0629 | 7.18 | 2.8 | 46 |
| 5[b] | 83.80879167 | −5.37296388 | ⋯ | ⋯ | −0.5351 | 0.8956 | 13.50 | −6.0 | 7 |

**Notes.**
[a] Identified by McBride & Kounkel (2019) as a source consistent with its origin from the Trapezium area.
[b] The Orion BN object is not observed by Gaia. Presented parameters are based on the Very Large Array observations (Rodríguez et al. 2017).

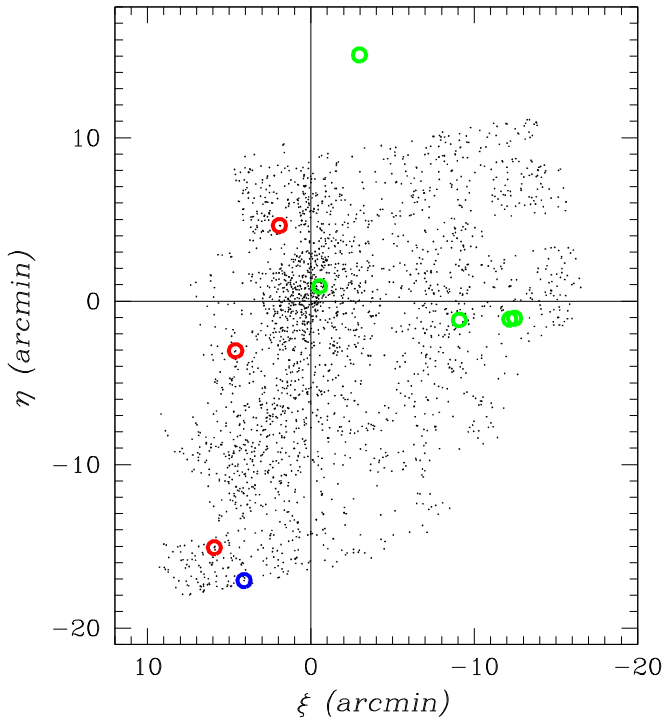


**Figure 10.** Spatial distribution of candidate ONC runaways. The background objects are the same as in Figure 3 but shown in tangential coordinates $\xi$, $\eta$. Runaways are divided into three parts: (1) confirmed by HST proper motions the likely da Rio et al. (2012) photometric low-mass members of the ONC (red circles); (2) an additional candidate from the HST proper motions (blue); and (3) selected candidates from the Gaia DR 2 catalog (green). The nearest runaway to the Trapezium is the BN object, neither detected by HST nor by Gaia but also marked in green.

runaways is between 10 and 19 km s$^{-1}$. It is surprising that we did not find any faster-moving objects. This tells us that there might be just a single scenario that is producing them.

The average velocity of this sample is ∼16 km s$^{-1}$, equivalent to 8.0 mas yr$^{-1}$. If we assume an angular distance of 20′ from the Trapezium and allow our sample to move at this velocity, then it takes ∼150,000 yr to cover this distance. Assuming that, out to 20′, there are ∼5 genuine runaways, and the age of ONC is ∼2 Myr, this would result in ∼70 lost sources with a mass less than 1 $M_\odot$. Considering the estimated total number of cluster members at ∼2800 (Hillenbrand & Hartmann 1998), this appears to be a minor ∼3% loss of the ONC members and, thus, would be a negligible correction to the mass function of the ONC.

## 4. Conclusions

We derived a new proper-motion catalog for low-mass stars and other sources in the area of the ONC using HST ACS/WFC observations over an 11 yr time span. The resulting catalog of relative proper motions contains 2454 objects in the magnitude range of $14.2 < m_{\rm F775W} < 24.7$. A subset of sources with high-precision proper motions is used to estimate the IVD of the ONC. The same subset also reveals the presence of three new low-mass candidate runaway sources, a result that is supported by extensive analysis of the candidate ONC runaways with a likely origin from the Trapezium.

In summary, our main findings are as follows.

1. We provide a detailed account of how to obtain reliable proper motions with HST in the area of the ONC that is otherwise notoriously difficult for astrometric studies.
2. We estimated the IVD of the ONC in two ranges of magnitude and for some distinctive spatial features in the area of the ONC. At the level of the achieved precision, the IVD appears to be nearly constant over the FOV.
3. The calculated IVD in the area around the Trapezium ($\sigma_{v,x} = 0.94$ and $\sigma_{v,y} = 1.25$ mas yr$^{-1}$) matches closely the estimate by Jones & Walker (1988) but disagrees with that of Kim et al. (2019) at the 7% level. At this time, none of the available IVD estimates seem to be more reliable than the others. The Gaia DR 2 data cannot provide a reliable list of genuine ONC members that are decisively separated from the YSOs in Orion A. We suspect that the high value of $\sigma_{v,y}$ is due to our current inability to obtain a clean sample of ONC members.
4. Using the HST ACS/WFC data alone, we identified three new faster-moving low-mass sources with likely origins in the Trapezium. In addition, one more candidate runaway is identified in Gaia DR 2. Altogether, the current census of the ONC candidate runaways is 10 sources covering a wide range of apparent magnitudes. Our analysis indicates that the number of bona fide runaways might be lower, and their impact on the observed ONC mass function appears to be insignificant.

The authors gratefully acknowledge grant support from programs GO-10246 and GO-13826, provided by NASA through grants from the Space Telescope Science Institute, which is operated by the Association of Universities for Research in Astronomy, Inc., under NASA contract NAS 5-26555. We thank Terrence Girard for his expert opinion on IVD and Marina Kounkel for sharing the main data on their selection of runaways. We also thank an anonymous referee for the

insightful review of our manuscript. This work has made use of data from the European Space Agency (ESA) mission Gaia (https://www.cosmos.esa.int/gaia), processed by the Gaia Data Processing and Analysis Consortium (DPAC, https://www.cosmos.esa.int/web/gaia/dpac/consortium). Funding for the DPAC has been provided by national institutions, in particular, the institutions participating in the Gaia Multilateral Agreement.

*Facility:* Hubble Space Telescope.

## ORCID iDs

Imants Platais https://orcid.org/0000-0003-2599-2459
Massimo Robberto https://orcid.org/0000-0002-9573-3199
Andrea Bellini https://orcid.org/0000-0003-3858-637X
Mario Gennaro https://orcid.org/0000-0002-5581-2896
Giovanni Strampelli https://orcid.org/0000-0002-1652-420X
Selma E. de Mink https://orcid.org/0000-0001-9336-2825
David R. Soderblom https://orcid.org/0000-0002-0322-8161

## References

Allen, C., Costero, R., Ruelas-Mayorga, A., & Sánchez, L. J. 2017, MNRAS, 466, 4937
Anderson, J. 2007, Instrument Science Report ACS 2007-08 (Baltimore, MD: STScI)
Anderson, J., & King, I. R. 2006, Instrument Science Report ACS 2006-01 (Baltimore, MD: STScI)
da Rio, N., Robberto, M., Hillenbrand, L. A., Henning, T., & Stassun, K. G. 2012, ApJ, 748, 14
da Rio, N., Robberto, M., Soderblom, D. R., et al. 2010, ApJ, 722, 1092
da Rio, N., Tan, J. C., & Jaehnig, K. 2014, ApJ, 795, 55
Dzib, Sergio A., Loinard, Laurent, Rodríguez, Luis F., et al. 2017, ApJ, 834, 139
Gaia Collaboration, Brown, A. G. A., Vallenari, A., et al. 2016, A&A, 595, A2
Gaia Collaboration, Lindegren, L., Hernández, J., et al. 2018, A&A, 616, A2
Großschedl, J. E., Alves, J., Meingast, S., et al. 2018, A&A, 619, A106
Hillenbrand, L. A. 1997, AJ, 113, 1733
Hillenbrand, L. A., & Hartmann, L. W. 1998, ApJ, 492, 540
Indriolo, N., Tan, J. C., Boogert, A. C. A., et al. 2018, ApJL, 865, L18
Jones, B. F., & Walker, M. F. 1988, AJ, 95, 1755
Kim, D., Lu, J. R., Konopacky, Q., et al. 2019, AJ, 157, 109
Kounkel, M., Covey, K., Suárez, G., et al. 2018, AJ, 156, 84
Kozhurina-Platais, V., Borncamp, D., Anderson, J., Grogin, N., & Hack, W. 2015, Instrument Science Report ACS 2015-06 (Baltimore, MD: STScI)
Kozhurina-Platais, V., Grogin, N., & Sabbi, E. 2018, Instrument Science Report ACS/WFC 2018-01 (Baltimore, MD: STScI)
Kuhn, M. A., Hillenbrand, L. A., Sills, A., Feigelson, E. D., & Getman, K. V. 2019, ApJ, 870, 32
Luhman, K. L., Robberto, M., Tan, J. C., et al. 2017, ApJL, 838, L3
Mahmud, N., & Anderson, J. 2008, PASP, 120, 907
Manara, C. F., Beccari, G., da Rio, N., et al. 2013, A&A, 558, A114
Marschall, L. A., & Mathieu, R. D. 1988, AJ, 96, 1956
McBride, A., & Kounkel, M. 2019, ApJ, 884, 6
Megeath, S. T., Gutermuth, R., Muzerolle, J., et al. 2012, AJ, 144, 192
Meingast, S., Alves, J., Mardones, D., et al. 2016, A&A, 587, A153
Menten, K. M., Reid, M. J., Forbrich, J., & Brunthaler, A. 2007, A&A, 474, 515
Moyano Loyola, G. R. I., & Hurley, J. R. 2013, MNRAS, 434, 2509
Muench, A., Getman, K., Hillenbrand, L., & Preibisch, T. 2008, in Handbook of Star-forming Regions, Vol. 1: The Northern Sky, ed. B. Reipurth (San Francisco, CA: ASP), 483
O'Dell, C. R. 2001, ARA&A, 39, 99
O'Dell, C. R., Muench, A., Smith, N., & Zapata, L. 2008, in Handbook of Star-forming Regions, Vol. 1: The Northern Sky, ed. B. Reipurth (San Francisco, CA: ASP), 544
O'Dell, C. R., Poveda, A., Allen, C., & Robberto, M. 2005, ApJL, 633, L45
Platais, I., Lennon, D. J., van der Marel, R. P., et al. 2018, AJ, 156, 98
Platais, I., van der Marel, R. P., Lennon, D. J., et al. 2015, AJ, 150, 89
Portegies Zwart, S. F. 2016, MNRAS, 457, 313
Poveda, A., Allen, C., & Hernández-Alcántara, A. 2005, ApJL, 627, L61
Robberto, M., Soderblom, D. R., Bergeron, E., et al. 2013, ApJS, 207, 10
Rodríguez, L. F., Dzib, S. A., Loinard, L., et al. 2017, ApJ, 834, 140
Shultz, M., le Bouquin, J.-B., Rivinius, T., et al. 2019, MNRAS, 482, 3950
Tan, J. C. 2004, ApJL, 607, L47
Úbeda, L., Kozhurina, V., & Bedin, L. R. 2013, Instrument Science Report ACS 2013-03 (Baltimore, MD: STScI)
van Altena, W. F., Lee, J. T., Lee, J.-F., et al. 1988, AJ, 95, 1744
van der Marel, R. P., & Anderson, J. 2010, ApJ, 710, 1063
Wang, L., Kroupa, P., & Jerabkova, T. 2019, MNRAS, 484, 1843